Biochimica et Biophysica Acta 1837 (2014) 880–887

Contents lists available at ScienceDirect

Biochimica et Biophysica Acta

journal homepage: www.elsevier.com/locate/bbabio

Development of a novel cryogenic microscope with numerical aperture of 0.9 and its application to photosynthesis research

Yutaka Shibata [a,*], Wataru Katoh [b], Tomofumi Chiba [a], Keisuke Namie [a], Norikazu Ohnishi [c], Jun Minagawa [c], Hanayo Nakanishi [b], Takumi Noguchi [b], Hiroshi Fukumura [a]

[a] Department of Chemistry, Graduate School of Science, Tohoku University, Aramaki aza Aoba, Aoba-ku, Sendai 980-8578, Japan
[b] Division of Material Science (Physics), Graduate School of Science, Nagoya University, Nagoya 464-8602, Japan
[c] Division of Environmental Photobiology, National Institute for Basic Biology, Okazaki 444-8585, Japan

ARTICLE INFO

Article history:
Received 10 January 2014
Received in revised form 5 March 2014
Accepted 10 March 2014
Available online 17 March 2014

Keywords:
Lateral heterogeneity of photosystem
Chlamydomonas reinhardtii
Photosystem I
Single-molecule spectroscopy
Fluorescence blinking

ABSTRACT

A novel cryogenic optical-microscope system was developed in which the objective lens is set inside of the cryostat adiabatic vacuum space. Being isolated from the sample when it was cooled, the objective lens was maintained at room temperature during the cryogenic measurement. Therefore, the authors were able to use a color-aberration corrected objective lens with a numerical aperture of 0.9. The lens is equipped with an air vent for compatibility to the vacuum. The theoretically expected spatial resolutions of 0.39 μm along the lateral direction and 1.3 μm along the axial direction were achieved by the developed system. The system was applied to the observations of non-uniform distributions of the photosystems in the cells of a green alga, *Chlamydomonas reinhardtii*, at 94 K. Gaussian decomposition analysis of the fluorescence spectra at all the pixels clearly demonstrated a non-uniform distribution of the two photosystems, as reflected in the variable ratios of the fluorescence intensities assigned to photosystem II and to those assigned to photosystem I. The system was also applied to the fluorescence spectroscopy of single isolated photosystem I complexes at 90 K. The fluorescence, assigned to be emitted from a single photosystem I trimer, showed an intermittent fluctuation called blinking, which is typical for a fluorescence signal from a single molecule. The vibronic fluorescence bands at around 790 nm were observed for single photosystem I trimers, suggesting that the color aberration is not serious up to the 800 nm spectral region.

1. Introduction

Combinations of the optical microscope technique with various fluorescence-spectroscopic techniques have become promising approaches to various biological investigations. This is especially the case for the investigation of photosynthesis, since in-situ fluorescence spectroscopic analyses offer much information directly related to the functions of photosynthetic pigment–protein complexes. Actually, microscope measurements of in-situ fluorescence spectra [1,2] and their temporal variations with a picosecond time resolution [3,4] have exerted a powerful impact on photosynthesis research. On the other hand, fluorescence microspectroscopy studies of living oxygenic photosynthetic organisms have had the problem of overlaps of a lot of spectral components, often resulting in ambiguous interpretations. Since oxygenic photosynthesis is managed through the cooperation of a wide variety of pigment–protein complexes [5], the coexistence of many fluorescence spectral components is inherent to such organisms.

It has long been known that the problem of spectral overlap can be reduced by conducting experiments at cryogenic temperatures. In general, decreasing the temperature results in a drastic sharpening of the fluorescence spectrum of each component, leading to a much improved spectral resolution. From the fluorescence spectrum of a living leaf taken at room temperature, it is almost impossible to distinguish between the fluorescence spectral components of photosystem I (PS I) and photosystem II (PS II). In contrast, a leaf at 77 K typically shows the fluorescence spectrum of the PS II component, with a double-peaked band at 686 nm and 695 nm, which is clearly distinct from that of the PS I component, which shows a specific red-shifted band at around 710 to 735 nm depending on the organisms [6,7]. We know that the two peaks at 686 nm and 695 nm of the PS II component mainly come from the chlorophylls (Chls) bound to its core–antenna complexes, CP43 and CP47, respectively [8–11]. Another benefit of microspectroscopy at a low temperature is much milder photodamage to samples by high-intensity laser irradiation. Additionally, unwanted physiological responses of living samples can be suppressed at

Abbreviations: PS I, photosystem I; PS II, photosystem II; Chl, chlorophyll; RC, reaction center; NA, numerical aperture; APD, avalanche photodiode; CCD, charge-coupled device; LED, light-emitting diode; DM, n-dodecyl-β-D-maltoside; FWHM, full width at half maximum; PSF, point-spread function

* Corresponding author. Tel./fax: +81 22 795 6568.
E-mail address: shibata@m.tohoku.ac.jp (Y. Shibata).

http://dx.doi.org/10.1016/j.bbabio.2014.03.006
0005-2728/

low temperatures. This is extremely useful for observations of a biological sample because its fluorescence images in specific physiological states can be recorded without further perturbing the sample.

Another typical application of fluorescence microspectroscopy is single-molecule fluorescence spectroscopy, which has become a powerful tool to study conformational dynamics of photosynthetic pigment–protein complexes [12–18]. It is necessary to conduct experiments at cryogenic temperatures for fluorescence detection of a single photosynthetic reaction-center (RC) complex because the complex generally has a very low fluorescence quantum yield at room temperature due to the competing, extremely efficient charge-separation. PS I has a very low fluorescence quantum yield at room temperature, whereas it has a rather strong fluorescence emission below 100 K [14,19].

A drawback of cryogenic microspectroscopy is its limited spatial resolution. Basically, there are two methods of cryogenic microscopy. In one method, the objective lens is set inside the cryostat and immersed in the cooling medium [12,13,20]. On the other method, the lens is set outside the cryostat [21–23]. Since, in the former case, the microscope objective is cooled to a cryogenic temperature, one has to use a single lens made of fused quartz that has an extremely low heat-expansion coefficient. In this case, it is difficult to achieve an accurate color-aberration correction and a high numerical aperture (NA). In the latter case, one has to use an objective lens with a long working distance, again resulting in a limited NA. The NA of an objective lens used for cryogenic microspectroscopy hardly exceeds ca. 0.7. The limited NA of an objective lens results in not only a limited spatial resolution but also a limited collection efficiency of the fluorescence. Improvement of the collection efficiency of fluorescence is critical to the single-molecule fluorescence spectroscopy.

Here, we propose a novel cryogenic microscope set-up in which the objective lens is set inside the adiabatic vacuum space of the cryostat. This arrangement allows a drastically shortened working distance. Since the objective lens in this arrangement is adiabatically isolated from the cooled sample holder, we can use a semi-conventional objective lens composed of a set of glass lenses fixed inside a metal tube. Here, we use the word *semi-conventional* because the lens has to be equipped with an air vent for usage in the vacuum. This type of microscope has already been developed and applied in observations of solid surfaces [24]. However, no one has tried to develop it for observations of biological samples. Here, we demonstrate for the first time a high NA of 0.9 for measurements of biological samples at 90 K by the developed microspectroscopy system. The temperature can be further decreased to 10 K if liquid He is used as a cooling medium. Using the developed system, we reveal the non-uniform distributions of PS I and PS II inside a cell of a green alga, *Chlamydomonas* (*C.*) *reinhardtii*. We also demonstrate that the developed system is applicable to observations of the single-molecule fluorescence spectra of isolated PS I at 90 K. The improved spatial resolution of the developed system will be further applicable to the correlative microscopy, which is a recently emerging technique combining the cryo-electron tomography and the fluorescence microscopy ([25,26] and the references therein).

2. Materials and methods

2.1. Optical set-up

Fig. 1 is a schematic description of the developed cryogenic microscope. We adopted the inverted laser-scanning confocal microscope configuration. A home-built vacuum chamber contains an objective lens (Plan Apo HR100× NA0.9 custom-tailored for compatibility to the vacuum, Mitutoyo, Kawasaki), a piezo actuator (NS7120-C custom-tailored for compatibility to the vacuum, Nanocontrol, Tokyo) to control the fine focus, a hand-made copper sample holder, and a quartz stage (QS) to support the holder. The objective lens is designed for observation through a 0.3-mm-thick quartz cover slip. A sample solution is sealed in a cavity between two circular quartz plates (10-mm diameter) with a thickness of 0.3 mm. A Teflon spacer with a typical thickness of 0.05–0.2 mm is clipped between the quartz plates. The copper sample holder is fixed to the quartz sample stage through four rods made of thermally insulating polyphenylene sulfide (PPS) resin. The quartz stage is mounted on vacuum-compatible X–Y stages, and its position can be coarsely adjusted from outside of the chamber through the two right-angle arranged linear manipulators. The sample holder is connected to the cold head of the cryostat (Microstat, Oxford Instruments, Eynsham) through a copper braid to maintain the flexibility of the relative position of the holder with respect to the cold head. The bellows component allows the vertical movement of the bottom plate of the chamber fixing the objective lens. The focus can be coarsely adjusted by the vertical movement of the bottom plate.

Either a He–Ne laser (1137P, JDS Uniphase, Milpitas) or the second-harmonic generation light from a Ti:sapphire laser (MaiTai, Spectra-Physics, Mountain View) is used for the excitation light source. The excitation beam is reflected by a dichroic mirror and a pair of galvanic mirrors (VM500 plus, GSI, Bedford) and enters the objective lens through a quartz window at the bottom of the chamber. The lateral scanning of the focal point is carried out with the galvanic-mirrors. The fluorescence collected by the same objective lens passes in the opposite direction to the excitation beam, goes through the dichroic mirror, and is focused into the entrance slit of the polychromator (MS2004i, SOL instruments, Minsk). The fluorescence signal is detected with either an avalanche photodiode (APD) (id100-MMF50, ID Quantique, Geneva) or a liquid-nitrogen cooled charge-coupled device (CCD) camera (PyLoN:100BR eXcelon, Princeton Instruments, Trenton). The wavelength-dependent sensitivities of the system are estimated by measurements of the emission spectrum of a standard halogen lamp located at the sample position. As shown in Fig. S1, the sensitivity curve does not show any sharp wavelength dependence over the spectral range of interest. In the present study, therefore, we omitted the sensitivity correction.

The upper surface of the vacuum chamber is closed with a transparent acrylic window in order to maintain optical access from the upper side. A white light-emitting diode (LED) (MCWHL2-C3, Thorlabs, Newton) and a set of lenses and irises realizing the Kohler illumination are set over the acrylic window for measurements of a transmission image through the sample. When a transmission image is measured, the reflecting mirror is replaced with a half mirror, and the light through the sample is focused with an imaging lens onto a CMOS camera (Wraycam-G500, Wraymer Inc., Osaka).

2.2. Fluorescence beads spin-coated on a quartz surface

A suspension of fluorescence beads with a diameter of 200 nm (F-8807, Life Technologies Japan, Tokyo) was appropriately diluted with a 1% (w/v) polyvinyl alcohol aqueous solution. The solution was then spin-coated on a circular quartz plate with a thickness of 0.3 mm to obtain a thin film. The spinning rates were at 500 rpm for the initial 15 s and 2000 rpm for the following 60 s [27].

2.3. Sample preparation of C. reinhardtii living cells

Cells of wild-type *C. reinhardtii* strain 137c were grown in a Tris-acetate-phosphate (TAP) medium [28] under low light (~20 μmol photons m^{-2} s^{-1}). The concentration of the cells was adjusted by centrifugation and re-suspension to the culture medium. The culture medium was mixed with the same volume of glycerin to maintain the transparency of the solution and was sealed in the sample holder. The cells were incubated under dark for ca. 10 min and irradiated with PS I light (the white-LED light through a R72 long-pass filter, ~8 μmol photons m^{-2} s^{-1}) to induce state I. After the 10-min irradiation, the cooling process was started with a continuous liquid-nitrogen flow. The irradiation was continued until the sample temperature was below ca. 0 °C.

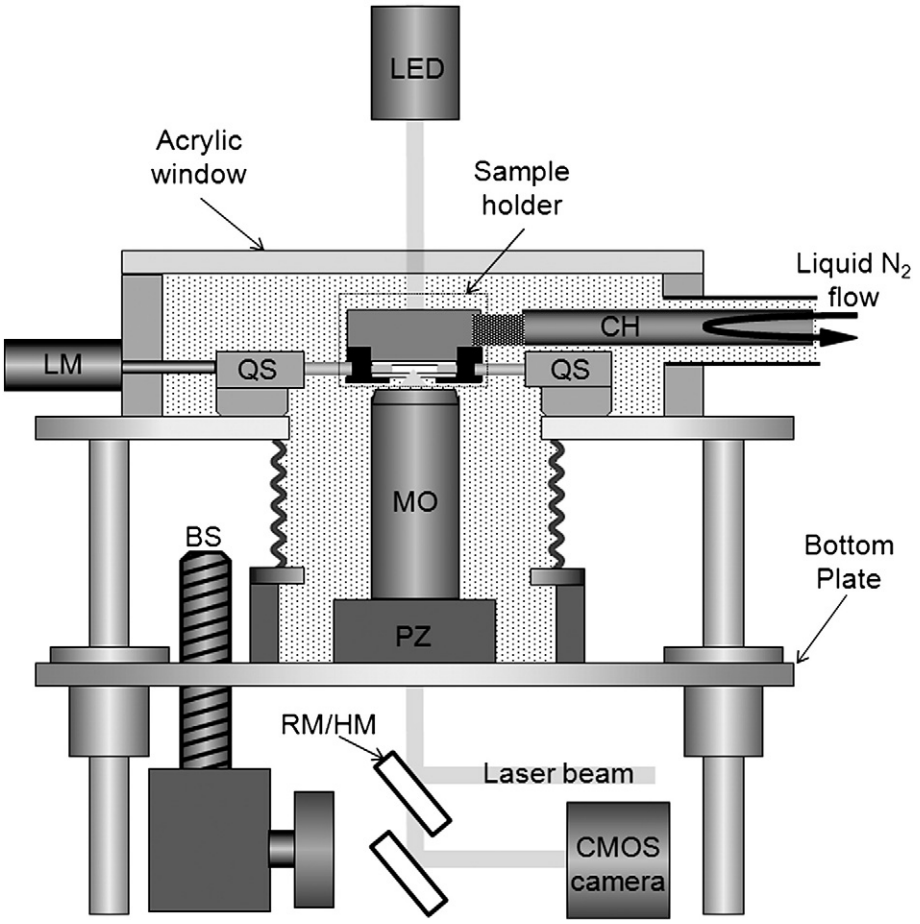

Fig. 1. Schematic view of the developed cryogenic microscope. LM: linear manipulator; QS: sample stage made of quartz; CH: cold head of the cryostat; MO: microscope objective; PZ: piezoelectric actuator; BS: ball-screw driving mechanism; LED: white light-emitting diode; RM/HM: reflecting mirror for the laser-scanning mode or half mirror for the transmission imaging mode. The shaded region indicates the adiabatic vacuum space.

2.4. Sample preparation of photosystem I isolated from Synechocystis sp. PCC 6803

Photosystem I (PS I) with histidine-tagged PsaL was purified from *Synechocystis* sp. PCC6803 (Kashino et al., unpublished) by Ni-affinity chromatography as described previously [29], with some modifications. Protein complexes were solubilized with 1% n-dodecyl-β-D-maltoside (DM), separated in buffer A (25% glycerol, 50 mM Hepes-NaOH, pH 7.8, 10 mM $MgCl_2$, 10 mM $CaCl_2$, 10 mM imidazole, 0.02% n-dodecyl-β-D-maltoside) using Ni-NTA super flow resin (Qiagen), and eluted with the buffer including 200 mM imidazole. The eluted PS I complexes were concentrated using a Vivaspin centrifugal filter unit (MWCO 100 kDa, Sartorius) and stored at −75 °C. The PS I complexes were diluted to various concentrations with a buffer (20 mM Tricine–HCl, pH 7.5) containing 25 mM $MgCl_2$, 5 mM sodium ascorbate, and 0.4 mM DM. For the single-molecule measurements, we used solutions with a PS I trimer concentration of 6.7 pM. The sample solution was sealed in the sample holder, incubated under dark for ca. 10 min, and cooled to 90 K.

3. Results and discussion

3.1. Evaluation of the spatial resolution

Fig. 2(A) shows a typical fluorescent bead image taken at 100 K using the He–Ne laser as the excitation source. The excitation power was 2 μW. To evaluate the full width at half maximum (FWHM) of the point-spread function (PSF) along the lateral direction, we fitted the obtained bead images to 2-dimensional (2-D) Gaussian functions,

$$Fl(x,y) = A_0 + A\exp\left[\frac{-1}{2(1-cor^2)}\left\{\left(\frac{x-x_0}{\sigma_x}\right)^2 + \left(\frac{y-y_0}{\sigma_y}\right)^2 - \frac{2cor(x-x_0)(y-y_0)}{\sigma_x\cdot\sigma_y}\right\}\right]. \quad (1)$$

The averaged FWHM of the PSF at a given axial displacement of the objective lens was then estimated according to the relation, $2\sqrt{\ln 2\cdot\sigma_x\sigma_y}$. As shown in Fig. 2(B), the averaged FWHM (open triangles) and the amplitude, *A* (open circles), of the 2-D Gaussian for the bead shown in panel (A) were plotted against the axial displacement (de-focus) of the objective. We fitted the amplitude vs. de-focus plot to a Gaussian function to determine the FWHM of PSF along the optical axis. According to the above procedure, the lateral and axial resolutions of the developed system were estimated to be 0.39 μm and 1.3 μm, respectively. These values are quite consistent with the theoretical ones, 0.38 μm and 1.4 μm, calculated by the convolution of the theoretical PSF with a uniform pigment distribution within a spherical bead with a diameter of 200 nm. Here, the theoretical PSF was calculated assuming the excitation at 633 nm and the emission at 680 nm, without the confocal pinhole.

3.2. Distributions of PS I and PS II in living C. reinhardtii cells

Fig. 3 shows typical fluorescence images of a *C. reinhardtii* cell with an excitation wavelength at 440 nm at 94 K. The excitation power was

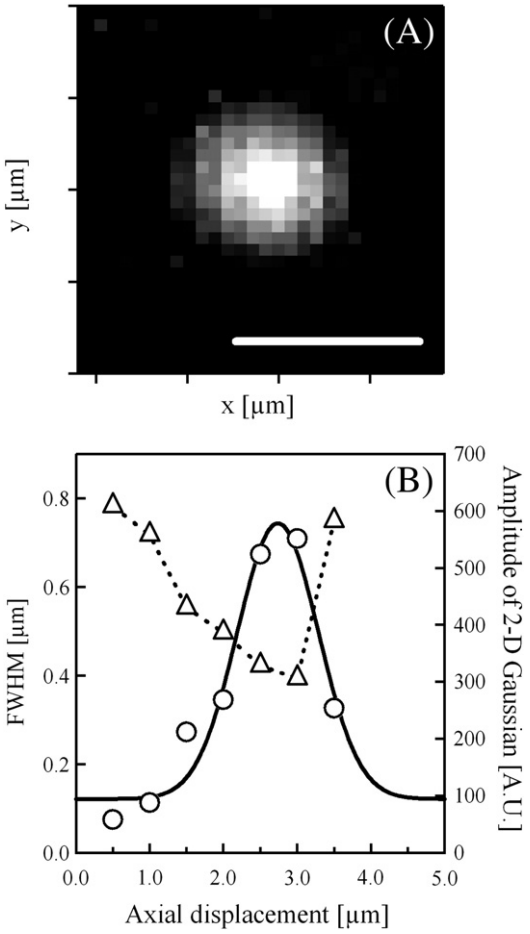

Fig. 2. (A) A typical fluorescence microscope image of a fluorescent bead with a diameter of 200 nm. The scale bar represents 1 μm. (B) The averaged FWHMs (open triangles, left axis) and the amplitudes (open circles, right axis) of the 2-D Gaussian obtained by the fitting, plotted against the axial displacement of the objective lens. The solid line is the fitting curve of the amplitude-axial displacement plot to a Gaussian. The dashed curve is a guide for the eyes.

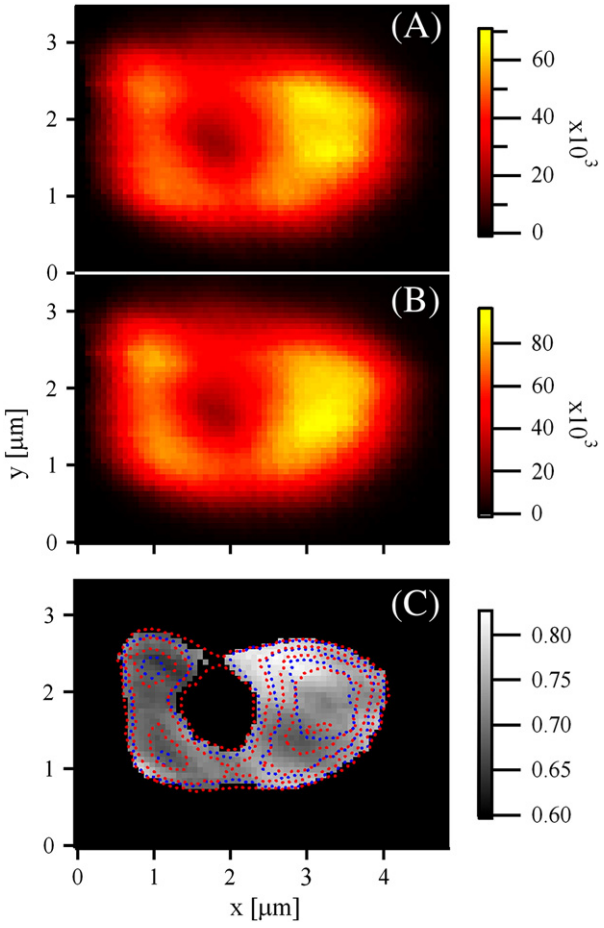

Fig. 3. Typical fluorescence microscope images of a *C. reinhardtii* cell at 94 K monitored in the PS II spectral region (680–690 nm) (A) and in the PS I region (710–720 nm) (B). Fluorescence-ratio map of the intensities in the PS II region to those in the PS I region (C). The contours of $Fl_{PS\ II}$ in panel (A) and $Fl_{PS\ I}$ in panel (B) are projected in panel (C) as the blue and red dotted lines, respectively.

250 nW at the sample position, corresponding to a power density of 200 W/cm^2 given the beam diameter of 0.39 μm. The images were reconstructed by using the fluorescence signal integrated over 680–690 nm (A) and over 710–720 nm (B). The former was mainly emitted from PS II and is designated hereafter as $Fl_{PS\ II}$, while the latter was from PS I and is designated hereafter as $Fl_{PS\ I}$. The thylakoid in the chloroplast appears as a bright region on the right, while the nucleus and the surrounding cytosol appear as a dark region on the left. Therefore, the axis from the apical side, where the flagella extend, to the basal side is probably oriented from left to right on these images. The pyrenoid, a subcellular micro-compartment localized in the basal region within the chloroplast, is not clearly visible in Fig. 3, probably due to the limited axial resolution and/or its insufficient development. Fig. 3(C) shows the fluorescence-ratio map of $Fl_{PS\ II}$ (panel A) to $Fl_{PS\ I}$ (panel B). Each pixel in Fig. 3(C) contains the ratio $Fl_{PS\ II}/Fl_{PS\ I}$ of the corresponding pixels in panels (A) and (B), except for those in which signals are less than a certain threshold level as,

$$\text{ratio} = \frac{Fl_{PS\ II}}{Fl_{PS\ I}} \times \theta((Fl_{PS\ I} + Fl_{PS\ II}) - \text{threshold}). \quad (2)$$

Here, $\theta(x)$ is the Heaviside-step function which gives zero/unity for negative/positive x. The threshold value was defined to cut-off non-chloroplast regions in a ratio map. The blue and red dotted lines in Fig. 3(C) are the contour projections of $Fl_{PS\ II}$ in panel (A) and $Fl_{PS\ II}$ in panel (B), respectively. Fig. 3(C) clearly shows a non-uniform distribution of the $Fl_{PS\ II}/Fl_{PS\ I}$ ratio within a single cell.

To investigate the non-uniform ratio map in Fig. 3(C) in more detail, we made a Gaussian-decomposition analysis of the fluorescence spectra at all the pixels in the image. In the first stage, we carried out a global fitting of 15 spectra at randomly selected pixels in the image to fitting curves of the sum of five Gaussian functions. Here, the number of Gaussian functions was set to five according to previous reports [30,31]. The spectra were plotted against wavenumber as shown in Fig. 4. In this stage, the center wavenumber and the width of each component were the global parameters shared by the 15 spectra, whereas the amplitude of each Gaussian was set as a local parameter. In the second stage, we fitted all the spectra in the image to the sum of five Gaussian functions with the center wavenumbers and FWHMs fixed to the values obtained in the first stage. Fig. 4 shows the result of the first-stage fitting, in which the fitting curves in blue are in good agreement with the experimental curves in red. We can clearly distinguish the PS I and PS II components at around 14,000 cm^{-1} (714 nm) and at around 14,600 cm^{-1} (685 nm), respectively. The dotted lines show the spectra of the five Gaussian components. The obtained values of the center wavelength (the inverse of the center wavenumber) and the FWHM of each component are listed in Table 1 with their estimated standard-deviation values. The values in the table are basically consistent with those reported previously [30,31]. According to the assignments of the previous reports, component 1 at 679 nm mainly reflects the fluorescence from the peripheral antennae. Components 2 at 685 nm and 3 at 695 nm reflect

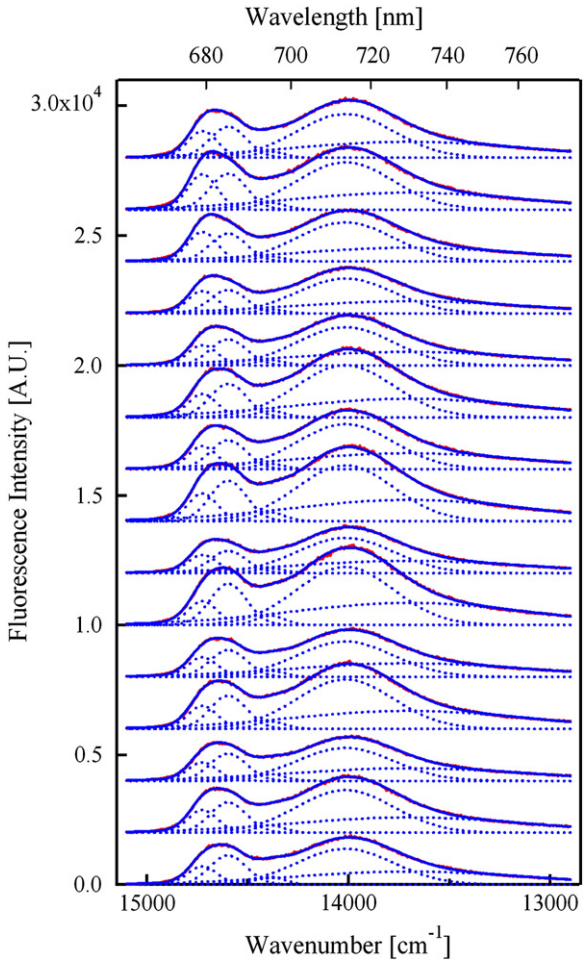

Fig. 4. Red curves show fluorescence spectra at 15 randomly selected positions of the *C. reinhardtii* cell shown in Fig. 3. Solid blue lines are the fitting curves to the sum of five Gaussian functions. Dotted blue lines show individual Gaussian component spectra.

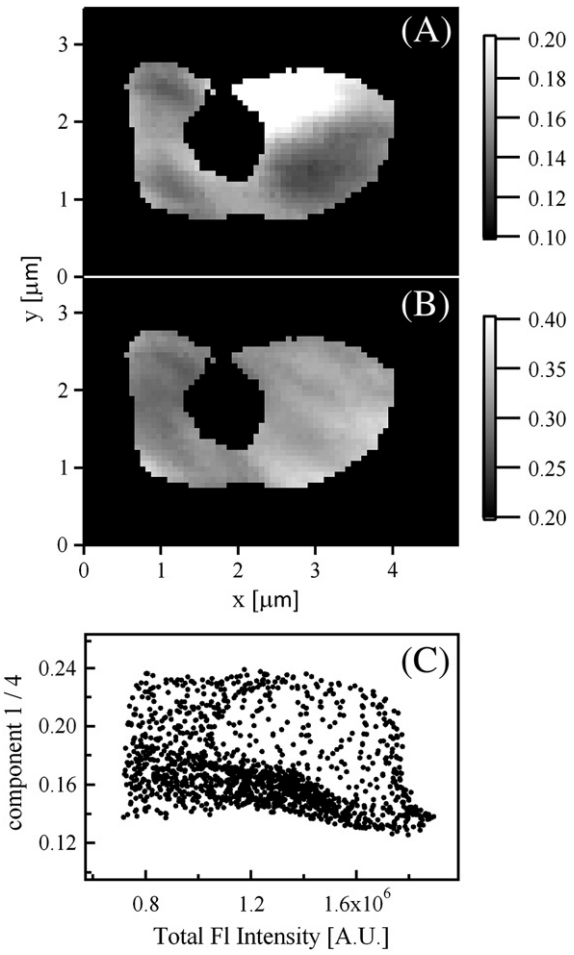

Fig. 5. Fluorescence-intensity ratio maps of the *C. reinhardtii* cell shown in Fig. 3. (A) Ratio map of the first to the fourth components and (B) that of the sum of the second and third components to the fourth component. The ratio values of the first to the fourth components are plotted against the sum of the intensities of the first to the fifth components (C).

the fluorescence peaks from CP43 and CP47 in PS II [8–11], respectively. Component 4 at 714 nm comes from PS I [30,31].

The fluorescence image reconstructed using the intensity of each Gaussian component is shown in Fig. S2(A) to (C). Fig. 5(A) and (B) shows the fluorescence-ratio maps of the intensities of the peripheral antenna and the PS II core complex components, respectively, to those of the PS I component. Here, the PS II core complex component was calculated as the sum of the spectral areas of the second and third Gaussian components. Again, we set a threshold value for the calculation of the ratio to discriminate the pixels with low signals. Fig. 5 clearly reveals a more intense contrast for the ratio map of the peripheral antenna to the PS I component in panel (A) than that of the PS II to the PS I component in panel (B). Thus, the non-uniform ratio map shown in Fig. 3(C) seems to be mainly from the non-uniform distribution of the peripheral antenna.

We have to consider the re-absorption effect on the fluorescence spectra even at the single-cell level [1]. The effect may have a serious impact, especially on the estimation of the intensity of the peripheral-antenna component (the first one), located at the blue-edge region of the total fluorescence spectrum. To check whether the re-absorption effect induces an erroneous estimation of the ratio maps, we plotted in Fig. 5(C) the intensity ratio of the peripheral-antenna to the PS I component against the sum of the intensities of all five Gaussian components. We consider here the horizontal axis of Fig. 5(C) as a rough measure of the pigment concentration at the given pixel. Thus, points on the right-hand side of Fig. 5(C) will suffer more from the re-absorption effect due to the high pigment concentration. Basically, the points in Fig. 5(C) do not show any correlation, especially below the total fluorescence-intensity value of ca. 1.4×10^6. However, the ratio tends to become smaller with the increasing total fluorescence-intensity value in the region higher than ca. 1.4×10^6. Thus, we cannot ignore the possibility that the re-absorption effect to some extent resulted in an underestimation of the component 1/4 ratio. The low component 1/4 ratio in Fig. 5(A) on the right-hand side of the cell may be partly due to the re-absorption effect. The development of an appropriate procedure to correct the re-absorption effect is an important issue for future study.

We believe that the ratio map of the PS II to the PS I components shown in Fig. 5(B) is relatively free from the re-absorption effect. In *C. reinhardtii*, the appressed membrane structures of the thylakoid are

Table 1
Obtained parameters for the Gaussian decomposition fitting of *C. reinhardtii* cell.

	1st component	2nd component	3rd component	4th component	5th component
Peak position [nm]	679.2 ± 0.1	685.1 ± 0.1	695.1 ± 0.1	713.5 ± 0.02	729.9 ± 0.2
FWHM [cm^{-1}]	173.2 ± 1.4	215 ± 4.7	167.9 ± 4.5	563.8 ± 1.3	1368 ± 4

not as well-developed as those in the grana system of higher-plant chloroplasts [32]. Even so, preferential localizations of PS II in the appressed membrane regions have been reported for this species by using the immunogold labeling electron-microscope technique [33]. Although the spatial resolution of the present optical measurement is not adequate to resolve the lateral heterogeneity observed by the electron microscope, the observed non-uniformity in the PS II/PS I ratio map in Fig. 5(B) might correspond to the non-uniform distribution of the appressed membrane structures within the chloroplast.

3.3. Single-molecule fluorescence spectroscopy of isolated cyanobacterial PS I

Fig. 6 shows a typical fluorescence image of a PS I solution diluted to a concentration of 6.7 pM. The excitation was done by a 100-μW He–Ne laser at the sample position. The image was taken at 90 K and was reconstructed by using the fluorescence signal integrated over the 700–730-nm spectral range, which is known to be the main fluorescence band of cyanobacterial PS I at cryogenic temperatures. From the values of the protein concentration of 6.7 pM and the thickness of the observed volume equal to the axial resolution of 1.3 μm, we estimate that one will find on average 0.6 molecule of PS I per 10 μm × 10 μm observation area. Since the density of the spots in Fig. 6 is comparable to the above estimation, we believe that each bright spot in the image corresponds to a single PS I trimer. As shown in Fig. S3, experimental results with varying protein concentrations are also in line with our interpretation.

Fig. 7panels (A-2), (B-2), and (C-2) show typical temporal chases of fluorescence spectra of three individual single PS I trimers. Each spectrum was taken with an accumulation time of 1 s, and 120 consecutive spectra corresponding to a 120-s chase are stacked in the graph. The time-integrated spectrum shown in panel (A-1) has a main band at around 725 nm, whereas those in panels (B-1) and (C-1) have peaks at around 717 nm. The spectrum in panel (B-1) has an additional peak in the shorter wavelength side at around 675 nm. The fluorescence bands at around 680 nm and 710–725 nm are attributed to the emissions from the bulk Chl and the red Chl pools, respectively. Here, the red Chl pools are pigment groups that have excited-state energies substantially lower than those of ordinary (bulk) Chl. The red Chl pools are specific to PS I and are considered to be composed of dimeric or trimeric Chls. The red shift of the excited-state energy is considered to be induced by the strong excitonic coupling and mixing of a charge-transfer (CT) nature to their excited states [34,35]. The PS I monomer complex contains ca. 100 Chls. The light energy absorbed by one of those antenna Chls is partly quenched by P700 or P700 cation, and the residual is funneled into a red Chl pool at cryogenic temperatures. Therefore, the red Chl pools are the main fluorescence emitters in PS I at low temperatures. The number of the red Chl pools was estimated to be three to four, each containing two to three Chls [34,36,37]. Fig. 7 reveals that, even at 90 K, some single PSI trimers show strong emissions from the bulk Chls, while others do not.

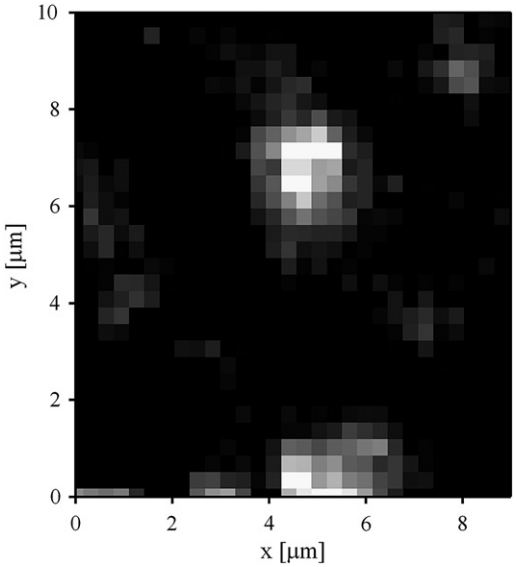

Fig. 6. Typical fluorescence microscope image of a 6.7-pM PS I solution at 90 K.

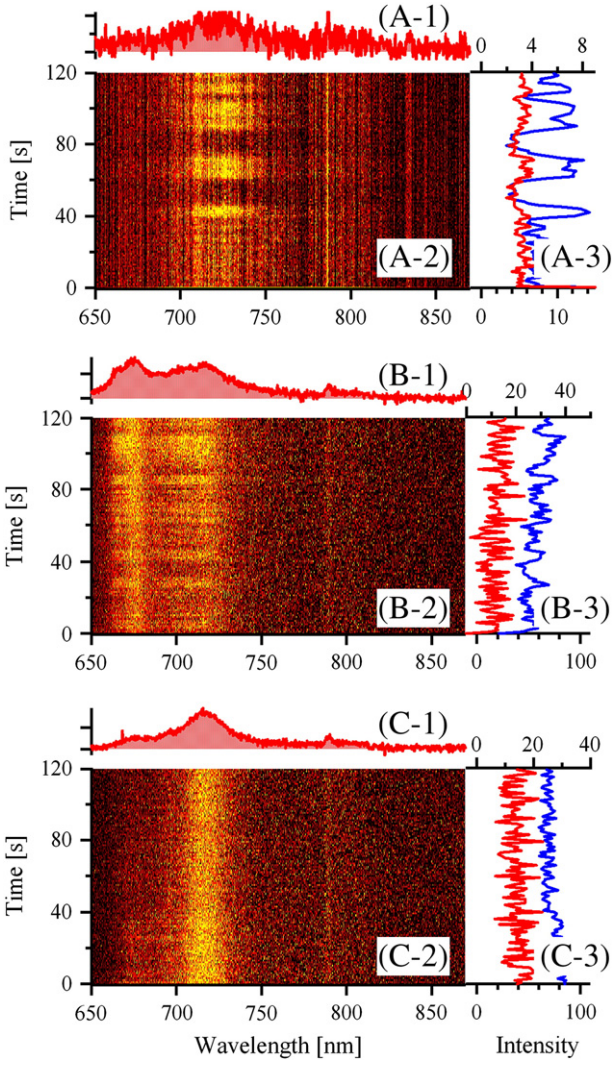

Fig. 7. Time-courses of and time-integrated fluorescence spectra of three single PS I trimers at 90 K. Each spectrum in panels (A-2), (B-2), and (C-2) is accumulated for 1 s and 120 consecutive spectra are stacked along the vertical axis. The time-integrated spectra over 120 s of the individual single PS I trimers are shown in panels (A-1), (B-1), and (C-1). Panels (A-3), (B-3), and (C-3) show the temporal changes in the intensities of the fluorescence bands integrated over the 710–730-nm range (blue, bottom horizontal scale) and the 790–810-nm range (red, top horizontal scale).

Blinking of the fluorescence, which is typical for a single molecule emission, was observed for the molecules shown in Fig. 7(A) and (B). To our knowledge, this is the first observation of the blinking of a single PS I fluorescence. The temporal changes of the fluorescence intensities in the 710–730-nm wavelength region are shown as blue lines on panels (A-3), (B-3), and (C-3). In the present preliminary study, fluorescence spectra of twelve PS I trimers were chased. Five out of the twelve molecules showed blinking behaviors, whereas the other seven showed fluorescence spectra without conspicuous intensity fluctuations as in Fig. 7(C). Among the five showing blinking, only the molecule shown in Fig. 7(A) exhibited a blinking with high contrast, in which the fluorescence intensity in the dark state dropped ca. 30% of the maximum level. On the other hand, although sudden changes of fluorescence intensity

were observed for other four molecules, the fluorescence intensity remained at 50 to 70% of the maximum during their dark states as in Fig. 7(B). The variable depth (contrast) of the blinking among individual molecules is consistent with the fact that PS I studied here forms a trimer. The complete bleach will be rare because it is realized only when all the three monomers turn to the dark state at the same time. The molecule in Fig. 7(A) exhibits three emitting states, i.e., dark (48–58 s and 77–85 s), medium bright (0–40 s), and bright (40–45 s, 60–70 s, 90–100 s, and 110–120 s). The dark, medium bright, and bright states may correspond to the situations with only one of the three monomers emitting, two of the three emitting, and all the monomers emitting, respectively.

The mechanism of the blinking of the fluorescence from the single PS I trimer is not clear at the moment. The primary candidate for the quenching state is the cationic form of P700, the primary electron donor of PS I [19]. The P700 cationic form has been known to be accumulated under a high irradiation condition as in the present experiment [38]. A slight conformational change in the protein surrounding both the red Chls and the bulk Chls may affect the overall excitation-energy pathway in the complex [17,39]. Thus, slight conformational fluctuations may cause the temporal modifications of the energy-transfer efficiency to the quenching state. It is known that, with an increase in temperature, the fluorescence quantum yield of PS I remains at the same level up to ca. 80 K but starts to decrease with further heating [15,19]. The blinking at 90 K may be related to the reported decrease of the fluorescence quantum yield. The temperature dependence of the blinking properties is an important issue for future study. Statistical properties of blinking, such as the distributions of the durations of bright and dark states, are of crucial importance to reveal the mechanism of blinking.

In Fig. 7(A-1), a week fluorescence band at around 800 nm is visible. This band can be assigned to a cluster of vibronic bands located ca. 1000 cm^{-1} lower than the 0–0 emission band at around 710–725 nm. In Fig. 7(A-3), we show the temporal fluctuations in the fluorescence intensity of the main band at around 720 nm (blue) and the vibronic band at around 800 nm (red). The intensity fluctuations of the two bands are clearly in phase, indicating that the weak fluorescence band at around 800 nm is not an artifact but a real signal. Thus, we demonstrate here that the developed cryogenic microscope system is applicable to the vibronic spectroscopy of single photosynthesis complexes [40], requiring a color-aberration-free objective lens over an expanded spectral range to near IR. Recently, Matsushita and co-workers have reported the development of a cryogenic microscope equipped with a reflection-type objective lens, which is almost free from color-aberration over a wide spectral range [41,42]. As shown in Fig. 7, our system maintains a comparable achromaticity to their system, at least in the 600-nm to 900-nm spectral region.

4. Conclusions

The developed cryogenic optical microscope set-up has enabled us to use an objective lens with a high NA of 0.9 at liquid nitrogen temperatures. The obtained spatial resolutions, 0.39 μm and 1.3 μm along the lateral and axial directions, respectively, almost achieved the theoretical limit. The system has been proven to be applicable to mapping the non-uniform distributions of PS I and PS II within a green algal cell and also to the fluorescence detection of a single PS I trimer. The color aberration was not serious up to the spectral range of 800 nm, allowing the detection of vibronic fluorescence bands of Chls bound to a single PS I.

Acknowledgements

We are grateful to Prof. Yasuhiro Kashino and Dr. Natsuko Inoue-Kashino at the University of Hyogo for kindly providing us the His-tagged PsaL strain of *Synechocystis* sp. PCC 6803. Y.S. and W.K. are deeply grateful to Mr. Masumi Katsuki at the Technical Center of Nagoya University for expert advice on the manufacture of the microscope system. This work was supported in part by Grants-in-Aid for Scientific Research (Nos. 21750017 and 24370060 to Y.S.), the 21st COE program for "the origin of the universe and matter" from the Japanese Ministry of Education, Culture, Sports, Science, and Technology (MEXT), and the Japan Society for the Promotion of Science (JSPS).

Appendix A. Supplementary data

Supplementary data to this article can be found online at http://dx.doi.org/10.1016/j.bbabio.2014.03.006.

References

[1] S. Kumazaki, M. Hasegawa, M. Ghoneim, Y. Shimizu, K. Okamoto, M. Nishiyama, H. Oh-Oka, M. Terazima, A line-scanning semi-confocal multi-photon fluorescence microscope with a simultaneous broadband spectral acquisition and its application to the study of the thylakoid membrane of a cyanobacterium *Anabaena* PCC7120, J. Microsc. 228 (2007) 240–254.
[2] W.F.J. Vermaas, J.A. Timlin, H.D.T. Jones, M.B. Sinclair, L.T. Nieman, S.W. Hamad, D.K. Melgaard, D.M. Haaland, In vivo hyperspectral confocal fluorescence imaging to determine pigment localization and distribution in cyanobacterial cells, Proc. Natl. Acad. Sci. U. S. A. 105 (2008) 4050–4055.
[3] K. Broess, J.W. Borst, H. van Amerongen, Applying two-photon excitation fluorescence lifetime imaging microscopy to study photosynthesis in plant leaves, Photosynth. Res. 100 (2009) 89–96.
[4] M. Iwai, M. Yokono, N. Inada, J. Minagawa, Live-cell imaging of photosystem II antenna dissociation during state transitions, Proc. Natl. Acad. Sci. U. S. A. 107 (2010) 2337–2342.
[5] L.Z. Taiz, E. Zeiger (Eds.), Plant Physiology, Sinauer Associates, Inc., Publishers, Sunderland, 2002.
[6] N. Murata, K. Satoh, in: Govindjee, J. Amesz, D.C. Fork (Eds.), Light Emission by Plant and Bacteria, Academic Press, Orlando, 1986, pp. 137–160.
[7] G.C. Papageorgiou, Govindjee (Eds.), Chlorophyll *a* Fluorescence: A Signature of Photosynthesis, Springer, Dordrecht, 2004.
[8] R.J. van Dorssen, J. Breton, J.J. Plijter, K. Satoh, H.J. Vangorkom, J. Amesz, Spectroscopic properties of the reaction center and of the 47 kDa chlorophyll protein of photosystem-II, Biochim. Biophys. Acta 893 (1987) 267–274.
[9] G.Z. Shen, W.F.J. Vermaas, Chlorophyll in a *Synechocystis* sp PCC-6803 mutant without photosystem-I and photosystem-II core complexes — evidence for peripheral antenna chlorophylls in cyanobacteria, J. Biol. Chem. 269 (1994) 13904–13910.
[10] M. Komura, Y. Shibata, S. Itoh, A new fluorescence band F689 in photosystem II revealed by picosecond analysis at 4–77 K: function of two terminal energy sinks F689 and F695 in PS II, Biochim. Biophys. Acta 1757 (2006) 1657–1668.
[11] Y. Shibata, S. Nishi, K. Kawakami, J.R. Shen, T. Renger, Photosystem II does not possess a simple excitation energy funnel: time-resolved fluorescence spectroscopy meets theory, J. Am. Chem. Soc. 135 (2013) 6903–6914.
[12] A.M. van Oijen, M. Ketelaars, J. Kohler, T.J. Aartsma, J. Schmidt, Unraveling the electronic structure of individual photosynthetic pigment–protein complexes, Science 285 (1999) 400–402.
[13] P. Tamarat, A. Maali, B. Lounis, M. Orrit, Ten years of single-molecule spectroscopy, J. Phys. Chem. A 104 (2000) 1–16.
[14] F. Jelezko, C. Tietz, U. Gerken, J. Wrachtrup, R. Bittl, Single-molecule spectroscopy on photosystem I pigment–protein complexes, J. Phys. Chem. B 104 (2000) 8093–8096.
[15] A.F. Elli, F. Jelezko, C. Tietz, H. Studier, M. Brecht, R. Bittl, J. Wrachtrup, Red pool chlorophylls of photosystem I of the cyanobacterium *Thermosynechococcus elongatus*: a single-molecule study, Biochemistry 45 (2006) 1454–1458.
[16] M. Brecht, H. Studier, A.F. Elli, F. Jelezko, R. Bittl, Assignment of red antenna states in photosystem I from *Thermosynechoccocus elongatus* by single-molecule spectroscopy, Biochemistry 46 (2007) 799–806.
[17] M. Brecht, V. Radics, J.B. Nieder, R. Bittl, Protein dynamics-induced variation of excitation energy transfer pathways, Proc. Natl. Acad. Sci. U. S. A. 106 (2009) 11857–11861.
[18] T.P.J. Kruger, E. Wientjes, R. Croce, R. van Grondelle, Conformational switching explains the intrinsic multifunctionality of plant light-harvesting complexes, Proc. Natl. Acad. Sci. U. S. A. 108 (2011) 13516–13521.
[19] M. Byrdin, I. Rimke, E. Schlodder, D. Stehlik, T.A. Roelofs, Decay kinetics and quantum yields of fluorescence in photosystem I from *Synechococcus elongatus* with P700 in the reduced and oxidized state: are the kinetics of excited state decay trap-limited or transfer-limited? Biophys. J. 79 (2000) 992–1007.
[20] S. Fujiyoshi, M. Fujiwara, M. Matsushita, Visible fluorescence spectroscopy of single proteins at liquid-helium temperature, Phys. Rev. Lett. 100 (2008).
[21] Y. Shibata, Y. Saga, H. Tamiaki, S. Itoh, Low-temperature fluorescence from single chlorosomes, photosynthetic antenna complexes of green filamentous and sulfur bacteria, Biophys. J. 91 (2006) 3787–3796.
[22] F. Vacha, V. Sarafis, Z. Benediktyova, L. Bumba, J. Valenta, M. Vacha, C.R. Sheue, L. Nedbal, Identification of Photosystem I and Photosystem II enriched regions of thylakoid membrane by optical microimaging of cryo-fluorescence emission spectra and of variable fluorescence, Micron 38 (2007) 170–175.
[23] Y. Shibata, W. Katoh, Y. Tahara, Study of cell-differentiation and assembly of photosynthetic proteins during greening of etiolated *Zea mays* leaves using confocal

fluorescence microspectroscopy at liquid-nitrogen temperature, Biochim. Biophys. Acta 1827 (2013) 520–528.
[24] M. Yoshimoto, J. Saraie, S. Nakamura, Impurity incorporation in epitaxially laterally overgrown GaN detected by cryogenic photoluminescence microscope with submicron spatial resolution, J. Cryst. Growth 237 (2002) 1075–1078.
[25] A. Sartori, R. Gatz, F. Beck, A. Rigort, W. Baumeister, J.M. Plitzko, Correlative microscopy: bridging the gap between fluorescence light microscopy and cryo-electron tomography, J. Struct. Biol. 160 (2007) 135–145.
[26] P.J. Zhang, Correlative cryo-electron tomography and optical microscopy of cells, Curr. Opin. Struct. Biol. 23 (2013) 763–770.
[27] A.M. van Oijen, M. Ketelaars, J. Kohler, T.J. Aartsma, J. Schmidt, Spectroscopy of individual light-harvesting 2 complexes of *Rhodopseudomonas acidophila*: diagonal disorder, intercomplex heterogeneity, spectral diffusion, and energy transfer in the B800 band, Biophys. J. 78 (2000) 1570–1577.
[28] D.S. Gorman, R.P. Levine, Cytochrome F and plastocyanin — their sequence in photosynthetic electron transport chain of *Chlamydomonas reinhardi*, Proc. Natl. Acad. Sci. U. S. A. 54 (1965) 1665–1669.
[29] H. Kubota, I. Sakurai, K. Katayama, N. Mizusawa, S. Ohashi, M. Kobayashi, P.P. Zhang, E.M. Aro, H. Wada, Purification and characterization of photosystem I complex from *Synechocystis* sp PCC 6803 by expressing histidine-tagged subunits, Biochim. Biophys. Acta 1797 (2010) 98–105.
[30] A. Murakami, Quantitative analysis of 77 K fluorescence emission spectra in *Synechocystis* sp. PCC 6714 and *Chlamydomonas reinhardtii* with variable PS I/PS II stoichiometries, Photosynth. Res. 53 (1997) 141–148.
[31] R. Morgan-Kiss, A.G. Ivanov, J. Williams, M. Khan, N.P.A. Huner, Differential thermal effects on the energy distribution between photosystem II and photosystem I in thylakoid membranes of a psychrophilic and a mesophilic alga, Biochim. Biophys. Acta 1561 (2002) 251–265.
[32] N.R. Bertos, S.P. Gibbs, Evidence for a lack of photosystem segregation in *Chlamydomonas reinhardtii* (Chlorophyceae), J. Phycol. 34 (1998) 1009–1016.
[33] O. Vallon, F.A. Wollman, J. Olive, Distribution of intrinsic and extrinsic subunits of the PS-II protein complex between appressed and non-appressed regions of the thylakoid membrane — an immunocytochemical study, FEBS Lett. 183 (1985) 245–250.
[34] V. Zazubovich, S. Matsuzaki, T.W. Johnson, J.M. Hayes, P.R. Chitnis, G.J. Small, Red antenna states of photosystem I from cyanobacterium *Synechococcus elongatus*: a spectral hole burning study, Chem. Phys. 275 (2002) 47–59.
[35] J. Adolphs, F. Müh, M.E.A. Madjet, M.S.A. Busch, T. Renger, Structure-based calculations of optical spectra of photosystem I suggest an asymmetric light-harvesting process, J. Am. Chem. Soc. 132 (2010) 3331–3343.
[36] L.O. Pålsson, J.P. Dekker, E. Schlodder, R. Monshouwer, R. van Grondelle, Polarized site-selective fluorescence spectroscopy of the long-wavelength emitting chlorophylls in isolated Photosystem I particles of *Synechococcus elongatus*, Photosynth. Res. 48 (1996) 239–246.
[37] Y. Shibata, A. Yamagishi, S. Kawamoto, T. Noji, S. Itoh, Kinetically distinct three red chlorophylls in photosystem I of *Thermosynechococcus elongatus* revealed by femtosecond time-resolved fluorescence spectroscopy at 15 K, J. Phys. Chem. B 114 (2010) 2954–2963.
[38] P. Setif, H. Bottin, Identification of electron-transfer reactions involving the acceptor-A1 of photosystem-I at room-temperature, Biochemistry 28 (1989) 2689–2697.
[39] M. Brecht, H. Studier, V. Radics, J.B. Nieder, R. Bittl, Spectral diffusion induced by proton dynamics in pigment–protein complexes, J. Am. Chem. Soc. 130 (2008) 17487–17493.
[40] F.P. Diehl, C. Roos, H.C. Jankowiak, R. Berger, A. Kohn, G. Diezemann, T. Basche, Combined experimental and theoretical study of the vibronic spectra of perylenecarboximides, J. Phys. Chem. B 114 (2010) 1638–1647.
[41] M. Fujiwara, S. Fujiyoshi, M. Matsushita, Single-component reflecting objective for ultraviolet imaging and spectroscopy at cryogenic temperature, J. Opt. Soc. Am. B 26 (2009) 1395–1399.
[42] M. Maruo, H. Inagawa, Y. Toratani, T. Kondo, M. Matsushita, S. Fujiyoshi, Three-dimensional laser-scanning confocal reflecting microscope for multicolor single-molecule imaging at 1.5 K, Chem. Phys. Lett. 591 (2014) 233–236.